Geochemistry Geophysics Geosystems G3
AN ELECTRONIC JOURNAL OF THE EARTH SCIENCES
Published by AGU and the Geochemical Society

Technical Brief
Volume 8, Number 11
16 November 2007
Q11004, doi:10.1029/2007GC001692
ISSN: 1525-2027

Methods for thermochemical convection in Earth's mantle with force-balanced plates

J. P. Brandenburg and P. E. van Keken
Department of Geological Science, University of Michigan, 2534 C.C. Little Building, Ann Arbor, Michigan 48109-1005, USA (jpbrande@umich.edu)

[1] Models of convection in the mantle can be used to study the effects of differentiation and remixing on the geochemical evolution of the Earth. Implementation of melting and degassing at mid-ocean ridges and subduction zones requires an adequate approximation of plate tectonics as well as temperature-dependent rheology. We have developed a new two-dimensional cylindrical model that combines a force-balance method for energetically consistent stiff plates with tracer-discretized chemical buoyancy. Basaltic crust is extracted at distinct spreading centers and is subducted into the lower mantle. We find that the unmodified implementation of the force-balance equations in a full cylinder causes occasional spurious rotations by amplification of numerical discretization errors. The method is stable if a single internal symmetry boundary condition is used, but this causes artificial pooling of dense crust near the boundary where it is easily disrupted. This results in artificially enhanced remixing of dense crust. We modify the force-balance equations to damp net lateral plate movement. The energetic consistency of this modification is then demonstrated by comparison to a one-plate, single convection cell calculation. With the removal of the symmetry boundary condition a more continuous rate of crustal pooling is observed. This suggests that models with symmetry boundary conditions may overpredict the rate of pooling and remixing of ancient crust.

Components: 4898 words, 8 figures, 3 tables.

Keywords: thermochemical convection; force-balanced plates; mixing.

Index Terms: 8120 Tectonophysics: Dynamics of lithosphere and mantle: general (1213); 8125 Tectonophysics: Evolution of the Earth (0325); 0545 Computational Geophysics: Modeling (4255).

Received 18 May 2007; **Revised** 18 September 2007; **Accepted** 26 September 2007; **Published** 16 November 2007.

Brandenburg, J. P., and P. E. van Keken (2007), Methods for thermochemical convection in Earth's mantle with force-balanced plates, *Geochem. Geophys. Geosyst.*, *8*, Q11004, doi:10.1029/2007GC001692.

1. Introduction

[2] The extraction of basalt crust at mid-ocean ridges is likely the main source of chemical variability in the Earth's mantle [*Silver et al.*, 1988; *Carlson*, 1994; *van Keken et al.*, 2002]. Numerical models of mantle convection can be used to study the chemical evolution of the Earth by following the differentiation and remixing of this crust and associated residuum [e.g., *Christensen and Hofmann*, 1994; *Xie and Tackley*, 2004]. It has been recognized that the high density of oceanic crust may lead to its pooling at the core-mantle boundary (CMB) [*Hofmann and White*, 1982]. In order to understand the dynamical consequences of this type of differentiation, it is preferable to use an approximation of plate tectonics with self-

consistently defined zones of crust formation (mid-ocean ridges) and recycling (subduction zones).

[3] In general, formulations for plate tectonics in dynamic models involve a combination of high viscosity lithosphere and some method to break the lithosphere into mobile segments. The simplest approach is to kinematically prescribe a segmented velocity boundary condition [e.g., *Gurnis and Davies*, 1986; *Davies*, 2002; *Tan et al.*, 2002]. Kinematically imposed plates have been used in models of thermochemical convection [*Christensen and Hofmann*, 1994; *Davies*, 2002, 2006; *Brandenburg and van Keken*, 2007]. Although the kinematic boundary condition has the potential to interfere with the energy balance and mixing dynamics of the model, the well-defined and predictable spreading centers enable the consistent extraction of basaltic crust. Alternatively, the rheology can be locally weakened as a proxy for faulted plate margins [*Zhong and Gurnis*, 1994; *Lenardic and Kaula*, 1994; *Han and Gurnis*, 1999; *Chen and King*, 1998; *Zhong et al.*, 2000]. With a more complex rheology, these weak zones may form self-consistently in response to accumulating strain or other non-Newtonian effects [*Tackley*, 1998; *Trompert and Hansen*, 1998; *Bercovici*, 2003; *Stein et al.*, 2004]. These methods have found application in thermochemical convection models as well [*Gaherty and Hager*, 1994; *Tackley and Xie*, 2002; *Ogawa*, 2003; *Xie and Tackley*, 2004; *van Thienen et al.*, 2004]. Each of these methods has some drawbacks. Velocities need to be prescribed in the kinematic models which in general will violate the energy balance for free convection (i.e., the kinematic boundary condition will tend to either brake or speed up the energetically correct free surface velocities). Spreading centers tend to be somewhat diffuse when complex rheologies are applied. In addition, the parameters in the complex rheology approach are often difficult to tune, leading to large changes in dynamic behavior over time [e.g., *Tackley and Xie*, 2002; *Xie and Tackley*, 2004].

[4] When modeling the complex and often nonlinear process of thermochemical convection, it is useful to minimize the number of unknown and tunable parameters. The simple kinematic plate approach can be modified to be increasingly more consistent with energy conservation. One approach is to scale the plate velocities for the conservation of mass [*Lowman and Jarvis*, 1995]. A second, and in our view preferred approach is to minimize traction on the base of the lithosphere (hereafter referred to as the "force-balance method") [*Gable et al.*, 1991; *King et al.*, 1992, 2002; *Lowman et al.*, 2001, 2003; *Monnereau and Quéré*, 2001]. This results in an energetically consistent model that reproduces many of the same features (such as localized slab-like downwellings) found in models with more exotic rheologies, but with far fewer tuning parameters. We present a new technique for modeling thermochemical convection based on the force-balance method which allows us to link the extraction of basaltic crust to a number of well defined zones of divergence between plates. We will also discuss the challenges of implementing this method in two-dimensional (2-D) cylindrical models (with naturally occurring periodic boundary conditions) for thermochemical convection with strongly temperature-dependent rheology.

2. Methodology

[5] We model the thermochemically convecting mantle as an incompressible Boussinesq fluid at infinite Prandtl number. For this, we solve the coupled mass-conservation, Stokes and heat advection-diffusion equations in nondimensional form. Respectively, these are

$$\nabla \cdot \mathbf{u} = 0 \tag{1}$$

$$-\nabla P + \nabla \cdot (\eta \dot{\underline{\epsilon}}) = [RaT - RcC]\hat{\mathbf{g}} \tag{2}$$

$$\frac{\partial T}{\partial t} + (\mathbf{u} \cdot \nabla)T = \nabla^2 T + Q \tag{3}$$

$\mathbf{u}$ is the velocity vector, P the dynamic pressure, t time, T the temperature and $\hat{\mathbf{g}}$ the unit vector in the direction of gravity. C is the chemical composition, η the nondimensional dynamic viscosity and Q is the volumetric internal heating. $\dot{\underline{\epsilon}}$ is the strain-rate tensor ($\nabla\mathbf{u} + \nabla\mathbf{u}^T$). Ra is the thermal Rayleigh Number:

$$Ra = \frac{\rho_o g \alpha_o \Delta T h^3}{\eta_o \kappa_o} \tag{4}$$

ρ_o is the reference density and κ_o is the reference thermal diffusivity. α_o is the average thermal expansivity and η_o is the average dynamic viscosity. For reference values, see Table 1. Rc is the compositional Rayleigh Number:

$$Rc = \frac{g \Delta \rho h^3}{\kappa_o \eta_o} \tag{5}$$

Table 1. Dynamic Variables and Reference Values

Quantity	Variable	Nondimensionalization
Length	l	$l' = lh'$
Time	t	$t' = t(h'^2/\kappa_o')$
Volumetric heat production	Q	$Q' = Q(k_o'\Delta T_o'/h'^2)$
Quantity	**Constant**	**Reference Value[a]**
Thickness (absolute)	h'	2885 km
Thermal diffusivity (average)	κ_o'	10^{-6} m^2/s
Viscosity (lower mantle)	η_o'	10^{22} Pa · s
Temperature contrast (absolute)	$\Delta T_o'$	3000 K
Thermal expansivity (surface)	α_o'	$3 \cdot 10^{-5}$ K^{-1}
Density (average)	ρ_o'	4500 kg/m^3
Thermal conductivity (surface)	k_o'	4.2 W/m · K
Quantity	**Dimensional Depth**	**Nondimensional Radius**
Earth surface	0 km	1.4292
Base of lithosphere	100 km	1.3843
Base of transition zone	670 km	1.1479
Core-mantle boundary	2885 km	0.4292

[6] These equations are solved with a finite element method based on the Sepran finite element methodology [*Cuvelier et al.*, 1986]. The model domain is that of a full 2-D cylinder (Figure 1). We rescale the core mantle boundary and other internal radii (Table 1) to account for the fact that in 2-D with the normal CMB radius the relative surface area of the core is much larger than that in the spherical Earth. This scaling leads to overall heat transfer properties that are much closer to that of the Earth than those of the unscaled 2-D cylinder or Cartesian geometry [*Vangelov and Jarvis*, 1994; *van Keken*, 2001]. Similarly, the volume fraction of recycled oceanic crust in these rescaled models will provide a quantitatively better approximation to that in the spherical Earth.

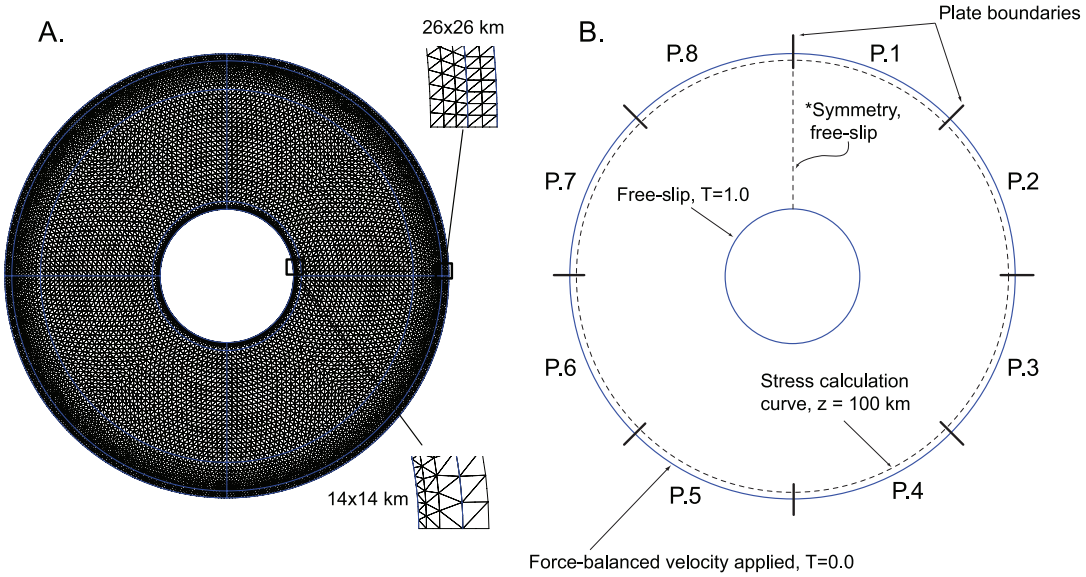

Figure 1. Model domain and setup: (a) The quadratic finite element mesh. (b) Diagram of boundary conditions, location of the stress calculation curve, and plate numbering convention (asterisk (*): vertical symmetry or connected (effectively periodic) boundary condition).

[7] The Stokes equations are solved on a two dimensional triangular mesh with quadratic elements, while the heat advection-diffusion equations are solved on a mesh with nested linear elements. A penalty function method is used to eliminate dynamic pressure from the Stokes equations. Compositional buoyancy is prescribed by the tracer method [*van Keken et al.*, 1997; *Tackley and King*, 2003] using a set of 474,172 tracers corresponding to an initial spacing of 10 km × 10 km. Tracers are advected by a fourth-order Runge-Kutta scheme [*van Keken et al.*, 1997]. The quadratic isoparametric elements have curved sides. To accurately determine velocity at the location of each tracer we use a Newton-Cotes iteration to obtain the values of the shape functions using the isoparametric mapping. Near the curved upper and lower surfaces, a cylindrical tracing formulation is used to assure that the tracers move parallel to the boundary. The heat equation is solved by an implicit second-order predictor-corrector method. Consequently, although we implement the Courant-Friedrichs-Levy (CFL) criterion (a stability criterion for explicit methods) to calculate the computational time step, this is not a requirement of our solution of the heat equation. Diffusion in the heat equation allows for the use of a larger time step. However, we do not explicitly model chemical diffusivity, so the advection of tracers requires a smaller time step than the heat equation. Therefore we advect tracers at 50% of the CFL time step with velocity fields interpolated between dynamic solutions computed at twice the CFL time step. Convergence tests performed on the full thermochemical solution and verification with benchmarks [*Blankenbach et al.*, 1989; *van Keken et al.*, 1997; *Lin and van Keken*, 2006] confirmed the accuracy of this method. For a detailed description of the thermochemical implementation, see *Brandenburg and van Keken* [2007].

[8] The model rheology has a moderate temperature and depth dependence:

$$\eta = \eta_r(z)\exp[-b(cT)] \quad \text{with} \quad \begin{cases} \eta_r(z) = 1000, c = 0, r > 1.3843 \\ \eta_r(z) = 1, c = 1, 1.3843 < r < 1.1479 \\ \eta_r(z) = 30, c = 1, r < 1.1479 \end{cases} \tag{6}$$

where $b = \ln(1000)$. The viscosity jumps at $r = 1.1479$ and $r = 1.3843$ represent the base of the lithosphere ($z = 100$ km) and the base of the transition zone ($z = 670$ km), respectively. We assume a constant plate thickness of 100 km and design the mesh so that a row of grid nodes is coincident with this depth. Stresses are calculated in each node, and total plate stress is calculated as a series of numerical integrals. In the thermochemical results shown here, we use 8 equal-sized plates (Figure 1). Each segment is assigned a speed consistent with the calculated stress. In practice, this is accomplished by superimposing scaled, purely kinematic test solutions for each plate onto a homogeneous (no-slip) solution for the Stokes equations. The scaling factor for each plate speed is computed by solution of the force-balance equations:

$$\begin{bmatrix} G_{1,1} & \cdots & G_{1,8} \\ \vdots & \cdots & \vdots \\ G_{8,1} & \cdots & G_{8,8} \end{bmatrix} \begin{bmatrix} v_1 \\ \vdots \\ v_8 \end{bmatrix} = \begin{bmatrix} \tau_1 \\ \vdots \\ \tau_8 \end{bmatrix} \tag{7}$$

where τ_i is the shear stress acting on plate i from the homogeneous solution, G_{ij} is the shear stress on plate j due purely to the motion of plate i (a nondimensional test speed of 1 is used), and v_i is the scaled plate speed. The kinematic plate solutions overlap by a width of 0.1 radians and are scaled by a linear ramp function. The sum of the ramped velocities in the overlapping region leads to a smooth velocity transition between plates with differential motion (Figure 2a). With stress calculated at the base of the lithosphere and the elimination of velocity discontinuities, the stress singularity found at fixed-points between plates in other studies disappears [*Gable et al.*, 1991]. This implementation has a very small dependence of plate speed on grid resolution in comparisons with published benchmark studies [*Koglin et al.*, 2005].

[9] In the cylindrical geometry (and Cartesian geometry with periodic boundary conditions), the test solutions are sensitive to modes that involve a component of rapid net-rotation. This is analogous to a solid rotation of the entire lithosphere, and is a highly unstable and spurious solution. Such solutions occur regardless of the choice of isoviscous, layered, or temperature-dependent rheologies. We think that these oscillations are enhanced in our models due to the nonalignment of the finite element grid with the variable direction of gravity in the cylindrical geometry. To eliminate this rotation we can impose a free-slip internal vertical boundary condition (hereafter the "vertical boundary condition"). Alternatively, the net-rotation can be suppressed by adding zero net-rotation con-

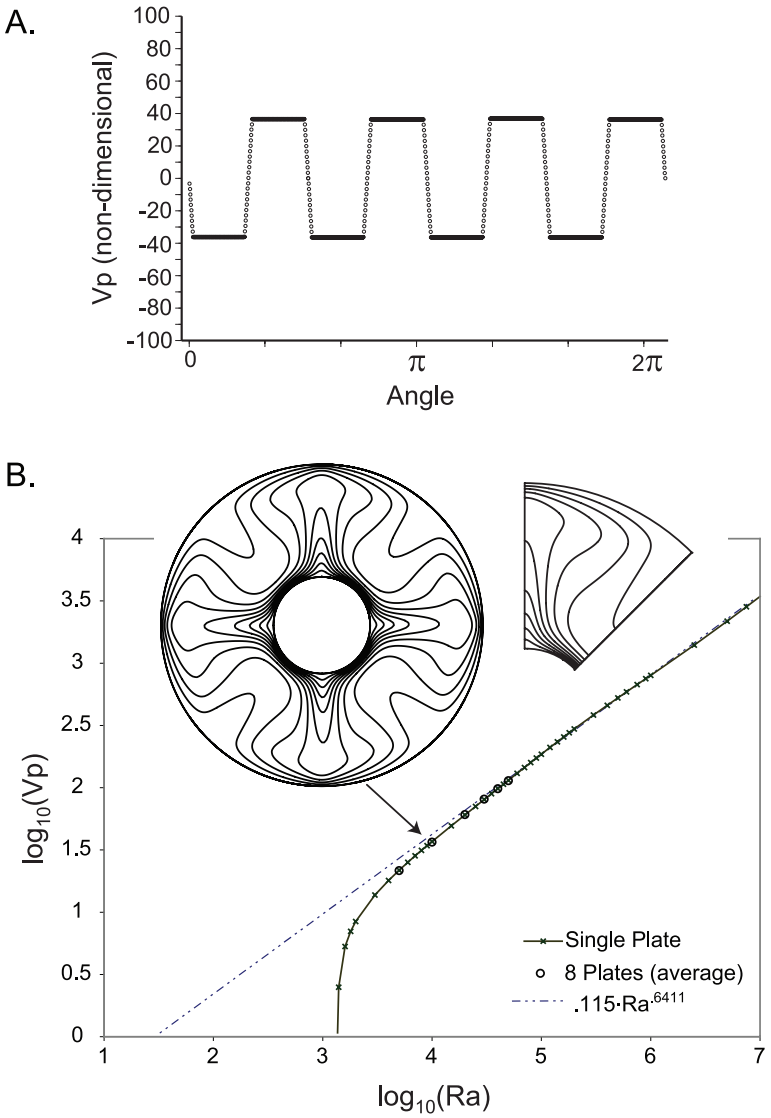

Figure 2. Steady state results: (a) Surface velocity from 8-plate benchmark model, Ra = 10^4. The surface position is given as an angle taken clockwise from "north." (b) Speeds from single plate and average plate speed from 8-plate steady state models. Isotherm plots (contour interval is 0.1) of the nondimensional temperature field for $Ra = 10^4$ results are superimposed.

straints to the force-balance equations. The modified system is

$$\begin{bmatrix} G_{1,1} & \cdots & G_{1,8} \\ \vdots & \cdots & \vdots \\ G_{8,1} & \cdots & G_{8,8} \\ 1 & \cdots & 1 \\ \vdots & \cdots & \vdots \\ 1 & \cdots & 1 \end{bmatrix} \begin{bmatrix} v_1 \\ \vdots \\ v_8 \\ 0 \\ \vdots \\ 0 \end{bmatrix} = \begin{bmatrix} \tau_1 \\ \vdots \\ \tau_8 \\ 0 \\ \vdots \\ 0 \end{bmatrix} \tag{8}$$

[10] Each of the additional rows states that the sum of the scaled plate velocities must be zero (hereafter the "zero net-rotation equation"). Since the system is overdetermined, calculation of an exact solution is no longer possible. Instead, an approximate solution must be calculated that best satisfies both stress and net-rotation constraints. We find an approximate solution by a least squares method. This results in a set of plate speeds that in some situations may still have a small component of net-rotation. Including the zero net-rotation equation multiple times biases the solution more strongly toward zero net-rotation.

[11] The extraction of basalt crust is simulated in melting zones connected to the plate boundaries. In

Table 2. Steady State Plate Velocities: 1 Plate

Ra	Vp
$5 \cdot 10^3$	21.675
$1 \cdot 10^4$	36.830
$2 \cdot 10^4$	60.197
$3 \cdot 10^4$	79.916
$4 \cdot 10^4$	97.706
$5 \cdot 10^4$	114.184

this way we link the zones of divergence established by the convective flow to zones of crust formation. Melting zones are established as a 100 km × 100 km region surrounding the boundary between any two plates with divergent motion. Any tracer passing vertically into a melting zone is moved to a random depth within a 10 km thick crustal layer [e.g., *Christensen and Hofmann*, 1994; *Davies*, 2002; *Brandenburg and van Keken*, 2007]. This mimics the formation of a basalt crust by 12.5% partial melting of mantle peridotite. The tracer-free layer created by this extraction is analogous to 90 km of depleted harzburgite. Tracer buoyancy is scaled so that the crust extracted is 10% denser than the ambient mantle (which results in $Rc = 0.1 \cdot Ra = 2 \cdot 10^5$). After subduction the basaltic crust carries this excess density by virtue of its higher concentration of tracers, while the depleted residuum has a slightly positive buoyancy. Any part of the mantle with the initial concentration of tracers has implicitly neutral chemical buoyancy.

3. Steady State Results

[12] At low convective vigor, computation of highly symmetrical steady state solutions in the full cylindrical model domain are possible. The symmetry of these solutions allows them to be decomposed into smaller model domains. For example, a solution with eight identical convection rolls will have exactly the same properties as any one of the rolls. We use this property to establish a plate speed benchmark for our model. The benchmark model domain is reduced from a full cylinder to a wedge with an angular extent of $\frac{\pi}{4}$. One force-balanced plate is imposed at the surface of the benchmark model. With only one plate, the force balance equation reduces to a 1 × 1 system, which can be solved analytically. In this restricted geometry, steady state solutions are possible across a wide range of convective vigor as determined by the value of *Ra*. Using the same depth- and temperature-dependent rheology as the thermochemical model but removing all internal heating and chemical effects (which tend to enhance time dependence) we varied *Ra* arbitrarily between 10^3 and $3 \cdot 10^7$ (Table 2). The plate speeds calculated in this range scaled as $V_p = .115Ra^{.6411}$, except for a systematic departure near the critical value of $Ra = 1.1 \cdot 10^3$ (Figure 2b).

[13] The benchmark model is reproducible by 8-fold symmetry in the full cylinder until *Ra* becomes sufficiently large for the onset of time dependence. We found that including the zero net-rotation equation at least once for each plate (each additional inclusion of the zero net-rotation equation adds a row, creating a 16 × 8 force-balance system in this case) was necessary to obtain steady state solutions. Exploration of the higher *Ra* time-dependent models revealed that small amounts of spurious rotation persisted when the force-balance system was smaller than 16 × 8. Therefore we adopt the 16 × 8 system for our thermochemical model. The plate velocities calculated in the steady state models are all within 5% of the one-plate model predictions, while the average plate speed agrees to within 1% (Figure 2b). Including the net rotation equation more than 8 times enhances the symmetry of the steady state solution and further reduces the spread of plate velocities (Table 3), but did not have a significant effect in time-dependent calculations. The close agreement between the 1-plate and 8-plate steady state results demonstrates the consistency of our expanded force-balance method with the energetics of convection.

4. Thermochemical Results

[14] Results from four thermochemical calculations are presented. Model 1a contains neutrally buoyant crust with a symmetry boundary condition, and Model 1b does the same with no symmetry boundary condition and our expanded force-balance equations. Models 2a and 2b are the same as 1a and 1b, respectively, except that both contain crust

Table 3. Steady State Plate Velocities: 8 Plates

Ra	ave. Vp	max. Vp	min. Vp	Dimension (M × N)
$5 \cdot 10^3$	21.54	21.87	21.29	16 × 8
$1 \cdot 10^4$	36.45	36.86	36.15	16 × 8
$2 \cdot 10^4$	60.70	61.53	60.09	16 × 8
$3 \cdot 10^4$	80.76	79.91	81.44	16 × 8
$4 \cdot 10^4$	98.02	96.67	99.19	16 × 8
$5 \cdot 10^4$	113.62	116.46	111.26	16 × 8
$5 \cdot 10^4$	113.70	115.23	112.52	32 × 8
$5 \cdot 10^4$	113.71	115.00	112.75	64 × 8

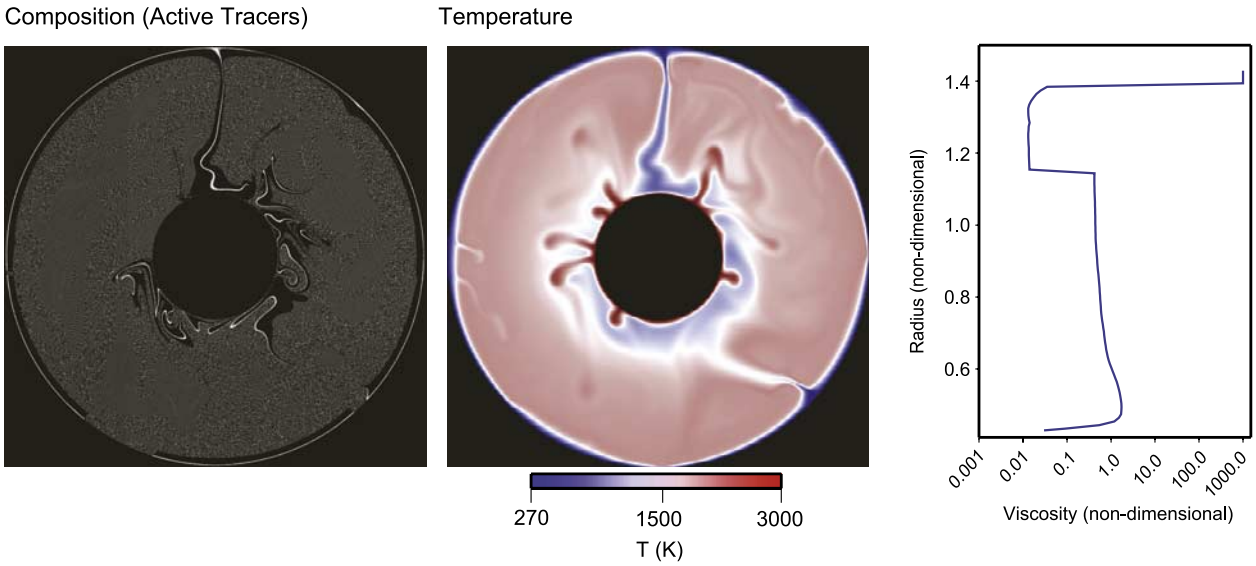

Figure 3. Snapshot of conditions 500 Ma after the start of the calculation for 1b (no vertical boundary condition). In the composition plot, basalt tracers are plotted as white pixels.

with 10% excess density. The present-day Bulk Silicate Earth heat production of $1.68 \cdot 10^{-8}$ W/m^3 translates to a nondimensional internal heating of Q = 11.1. We mimic the effects of present-day secular cooling (estimated at 50–100 K/Ba) by increasing the internal heating 50% to Q = 16.6. This results in a mantle that is heated mainly from within. Our choice of viscosity law parameters leads to an average nondimensional lower mantle viscosity of approximately 1.0 and an upper mantle

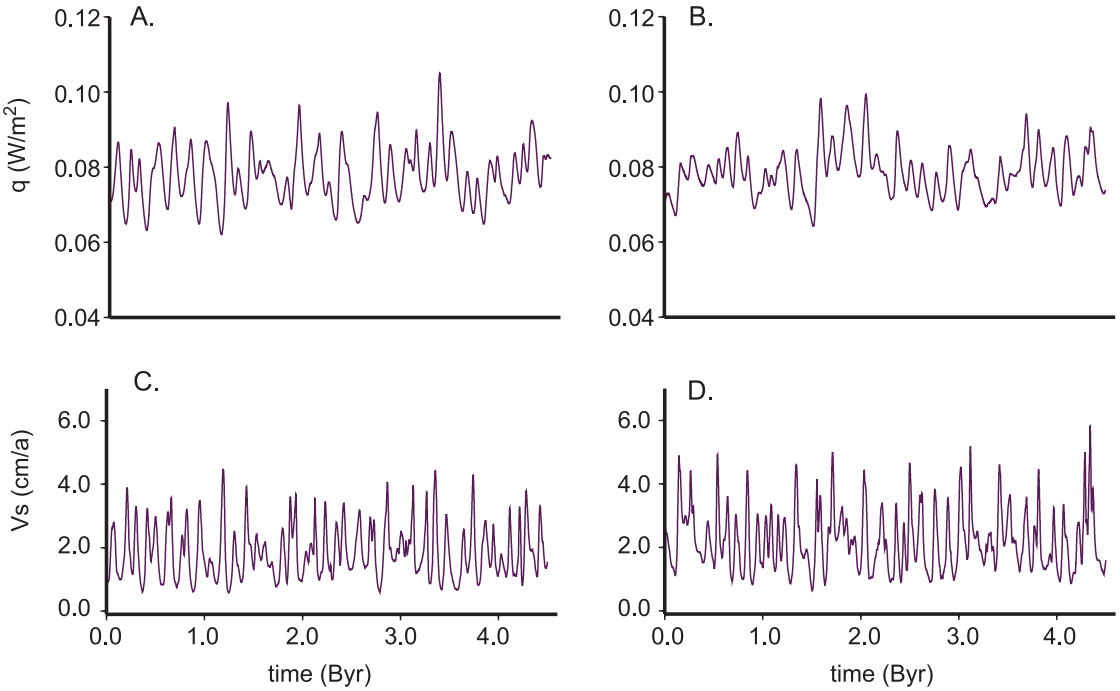

Figure 4. Time series of heat flow and average surface velocity for models with neutrally buoyant crust. Figures 4a and 4c are from model 1a (vertical boundary condition, standard force balance equations); Figures 4b and 4d are from model 1b (no vertical boundary condition, overdetermined force balance equations).

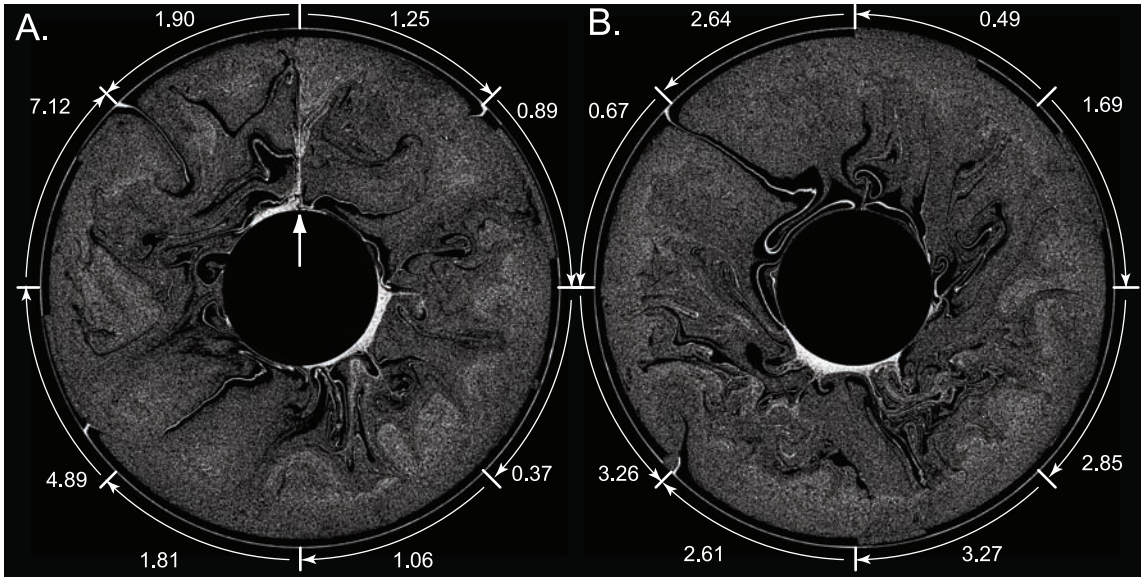

Figure 5. Composition at 2.0 Ba for (a) Model 2a and (b) Model 2b. The location of the vertical boundary condition is indicated with an arrow. The speed (in cm/a) and direction of motion are given above each plate.

viscosity of 0.01 (Figure 3). When dimensionalized by the values in Table 1, this yields a viscosity profile similar to that determined from inversion of post-glacial rebound data [e.g., *Mitrovica*, 1996; *Mitrovica and Forte*, 1997]. We find that the magnitude of lower mantle viscosity largely controls overall convective vigor. Taking the lower mantle average viscosity as the reference (approximately 10^{22} Pa · s) and the other characteristic reference values from Table 1, we calculate a thermal Rayleigh Number of order 10^6. However, the variability of dynamic parameters with depth is highly uncertain, particularly in the deep mantle. Variation in the estimates of mantle viscosity alone makes the calculation of *Ra* uncertain by at least an order of magnitude. Therefore we initially experimented with a variety of specific *Ra* values on the order of 10^6 and selected $Ra = 2 \cdot 10^6$ based on surface heat flow. To minimize the effects of transients, we started each model from an initial condition of fully developed flow and computed for at least 8 Ba to obtain suitable initial conditions for the thermochemical calculation. After this spin up period, the average surface velocity was approximately 2–3 cm/a corresponding to an average heat flow of approximately 80 mW/m^2 (Figure 4). The heat flow is consistent with values observed for the Earth's integrated geothermal heat flux [*Pollack et al.*, 1993]. The average surface velocity is slightly less than the present day tectonic average of approximately 5 cm/a [*Gordon*, 1998; *Bird*, 2003].

5. Discussion

[15] Although the results differ in detail, there are very few qualitative differences between models 1a and 1b. With neutrally buoyant crust, the mantle simply becomes progressively more heterogeneous. However, there are significant differences between 2a and 2b (Figures 5 and 6). After subduction, dense crust forms pools at the CMB in a manner similar to that seen in previous studies [*Christensen and Hofmann*, 1994; *Davies*, 2002; *Xie and Tackley*, 2004; *Brandenburg and van Keken*, 2007]. As these pools develop, they are swept aside by new slabs entering the lowermost mantle. Due to strong internal heating in these calculations, thermal plumes that develop from the CMB are fairly weak. This causes the pools of crust to develop a wide aspect ratio and irregular surface compared to "plume roots" that form in models with a stronger basal heating [e.g., *Christensen and Hofmann*, 1994; *Brandenburg and van Keken*, 2007]. The pools first appear approximately 500 Ma after the start of the calculation. However, the vertical boundary in 2a proves to be a source of continual disruption for any CMB structure. At any point in the calculation where there is not an active downwelling between plates P.1 and P.8, pooled

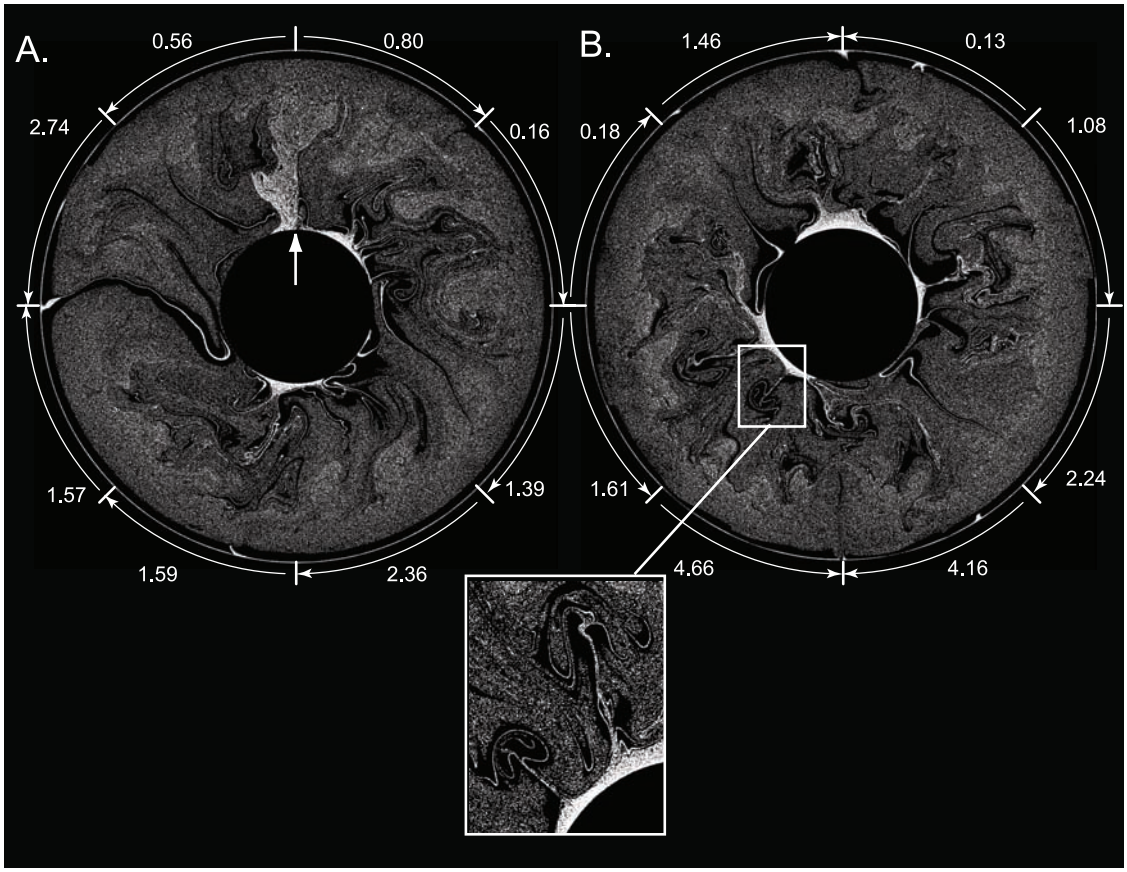

Figure 6. Composition at 3.6 Ba for (a) Model 2a and (b) Model 2b. The location of the vertical boundary condition is indicated with an arrow. The speed (in cm/a) and direction of motion are given above each plate. Inset is a reoriented close-up of two thermochemical plumes.

crust can be observed being swept back into the upper mantle along this boundary (Figure 5). Later in the calculation, the boundary becomes the site of large-scale disintegration of pooled crust (Figure 6). This type of wholesale disruption is not observed in 2b. To quantify these effects, we calculate the fraction of all dense tracers contained in the CMB pools [*Christensen and Hofmann*, 1994]. The

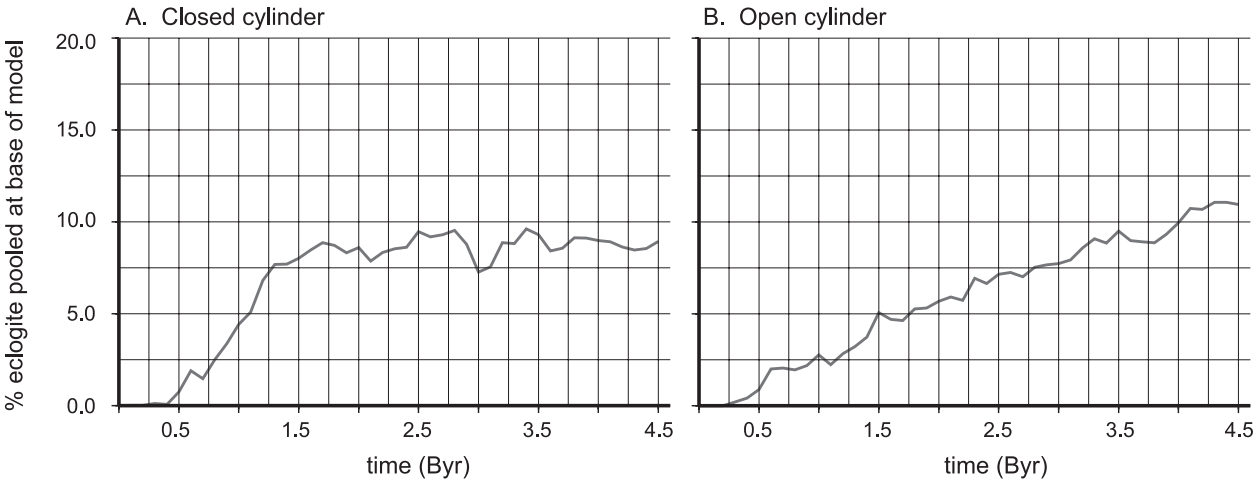

Figure 7. Fraction of dense tracers trapped in pools at the CMB for (a) Model 2a and (b) Model 2b. The effect of the vertical boundary condition can be seen in the truncation of the growth at 10% in Figure 7a.

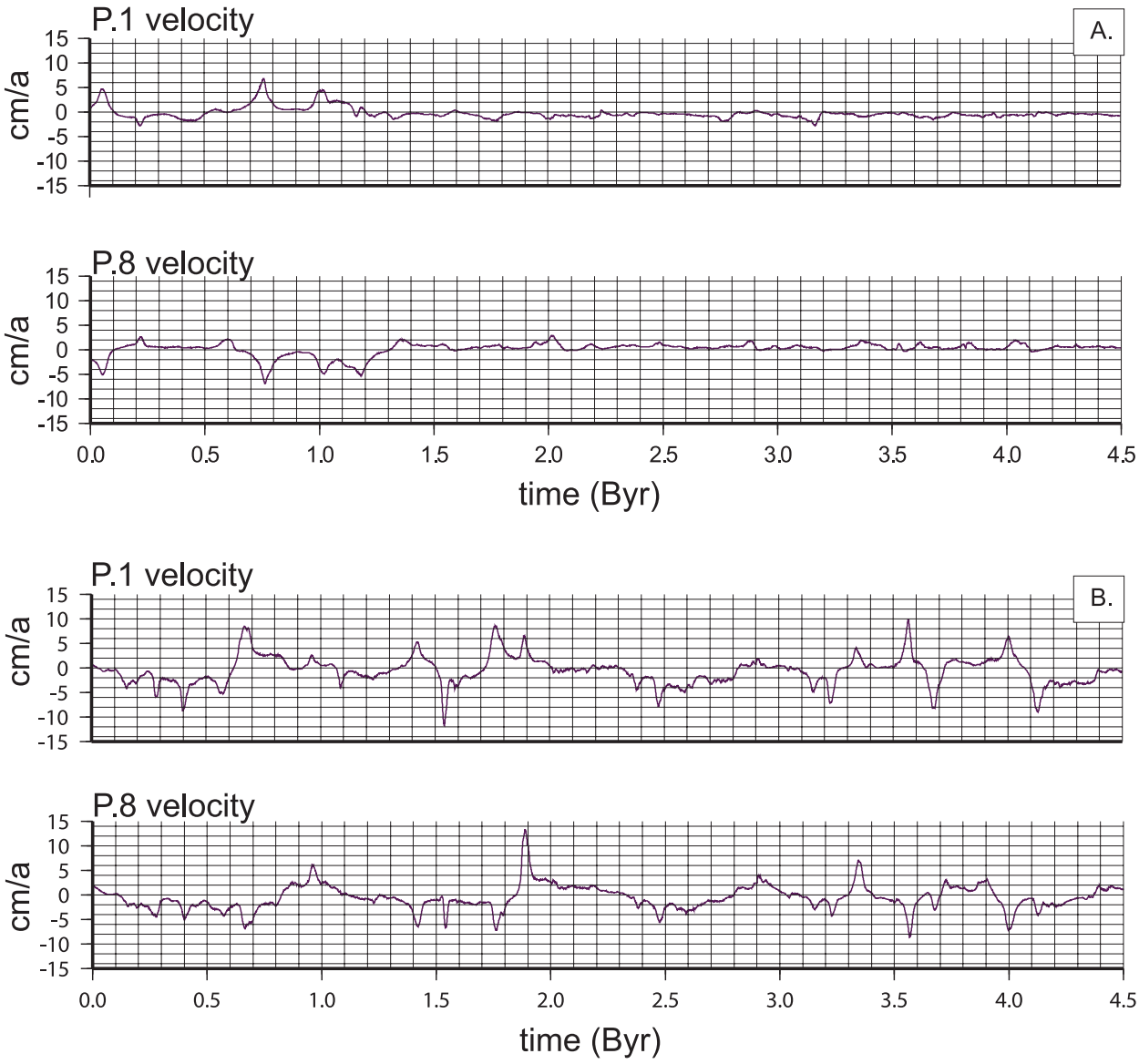

Figure 8. Speed for adjacent plates P.1 and P.8 from (a) 2a and (b) 2b. In Figure 8a, a large and persistent midmantle accumulation of dense tracers around the vertical boundary inhibits any differential motion between these plates after 1.5 Ba.

accumulation of crust proceeds with an initially greater rate in 2a, which is not unexpected given the enhanced stability provided by the vertical boundary (Figure 7). However, the disruption of the pools causes the accumulation to truncate at approximately 10%. The accumulation in 2b proceeds at a slower, but much more constant rate and eventually overtakes 2a. With the disruption of crustal pools, a large and fairly consistent accumulation of dense tracers forms in the midmantle around the vertical boundary in 2a. This accumulation feeds back into the differential motion of the overlying plates (P.1 and P.8). This denser mantle also has somewhat higher temperature. The result is an area of anomalous internal circulation that is somewhat independent from the general flow. This effectively eliminates any differential motion between P.1 and P.8 (Figure 8). No such behavior is observed in 2b.

6. Conclusions

[16] We have developed a new method for modeling thermochemical convection in the Earth's man-

tle by combining force-balanced plates with tracer-based density techniques. Basalt crust extracted at distinct spreading centers is subducted and when denser than the ambient mantle, forms pools at the CMB. When temperature-dependent viscosity is used in cylindrical geometry, the force-balance method has a tendency to rotate quickly between similar solutions. To damp this rotation, we test a vertical boundary condition and modifications to the force-balance equations. We verify that both methods yield qualitatively similar results when the crust is neutrally buoyant. However, we find that the presence of a vertical boundary condition artificially enhances the disruption of pooled crust at the CMB. Therefore models of thermochemical convection with these types of boundary condition may overestimate the remixing of such a layer [e.g., *Christensen and Hofmann*, 1994; *Xie and Tackley*, 2004; *Brandenburg and van Keken*, 2007].

Acknowledgments

[17] We thank Erik Kneller, Chris Ballentine, Erik Hauri, and Carolina Lithgow-Bertelloni for their helpful discussion and Carl Gable and an anonymous reviewer for their constructive reviews. This research was supported by the National Science Foundation.

References

Bercovici, D. (2003), The generation of plate tectonics from mantle convection, *Earth Planet. Sci. Lett.*, *205*, 107–121.

Bird, P. (2003), An updated digital model of plate boundaries, *Geochem. Geophys. Geosyst.*, *4*(3), 1027, doi:10.1029/2001GC000252.

Blankenbach, B., et al. (1989), A benchmark comparison for mantle convection codes, *Geophys. J. Int.*, *98*, 23–38.

Brandenburg, J. P., and P. E. van Keken (2007), Deep storage of oceanic crust in a vigorously convecting mantle, *J. Geophys. Res.*, *112*, B06403, doi:10.1029/2006JB004813.

Carlson, R. W. (1994), Mechanisms of Earth differentiation: Consequences for the chemical structure of the mantle, *Rev. Geophys.*, *32*(4), 337–361.

Chen, J., and S. D. King (1998), The influence of temperature and depth dependent viscosity on geoid and topography profiles from models of mantle convection, *Phys. Earth Planet. Inter.*, *106*, 75–92.

Christensen, U. R., and A. W. Hofmann (1994), Segregation of subducted oceanic crust in the convecting mantle, *J. Geophys. Res.*, *99*(B10), 19,844–19,867.

Cuvelier, C., A. Segal, and A. van Steenhoven (1986), *Finite Element Methods and the Navier-Stokes Equations*, Springer, New York.

Davies, G. F. (2002), Stirring geochemistry in mantle convection models with stiff plates and slabs, *Geochim. Cosmochim. Acta*, *66*(17), 3125–3142.

Davies, G. F. (2006), Gravitational depletion of the early Earth's upper mantle and the viability of early plate tectonics, *Earth Planet. Sci. Lett.*, *243*, 376–382.

Gable, C. W., R. J. O'Connell, and B. J. Travis (1991), Convection in three dimensions with surface plates: Generation of a toroidal flow, *J. Geophys. Res.*, *96*(B5), 8391–8405.

Gaherty, J. B., and B. H. Hager (1994), Compositional vs. thermal buoyancy and the evolution of subducted lithosphere, *Geophys. Res. Lett.*, *21*(2), 141–144.

Gordon, R. G. (1998), The plate tectonic approximation: Plate non-rigidity, diffuse plate boundaries, and global plate reconstructions, *Annu. Rev. Earth Planet. Sci.*, *26*, 615–642.

Gurnis, M., and G. F. Davies (1986), Mixing in numerical models of mantle convection incorporating plate kinematics, *J. Geophys. Res.*, *91*, 6375–6395.

Han, L., and M. Gurnis (1999), How valid are dynamic models of subduction and convection when plate motions are prescribed?, *Phys. Earth Planet. Inter.*, *110*, 235–246.

Hofmann, A. W., and W. M. White (1982), Mantle plumes from ancient oceanic crust, *Earth Planet. Sci. Lett.*, *57*, 421–436.

King, S. D., C. W. Gable, and S. A. Weinstein (1992), Models of convection-driven tectonic plates: A comparison of methods and results, *Geophys. J. Int.*, *109*, 481–487.

King, S. D., J. P. Lowman, and C. W. Gable (2002), Episodic tectonic plate reorganizations driven by mantle convection, *Earth Planet. Sci. Lett.*, *203*, 83–91.

Koglin, D. E.Jr., S. R. Ghias, S. D. King, G. T. Jarvis, and J. P. Lowman (2005), Mantle convection with reversing mobile plates: A benchmark study, *Geochem. Geophys. Geosyst.*, *6*, Q09003, doi:10.1029/2005GC000924.

Lenardic, A., and W. M. Kaula (1994), Tectonic plates, D″ thermal structure, and the nature of mantle convection, *J. Geophys. Res.*, *99*(B8), 15,697–15,708.

Lin, S.-C., and P. E. van Keken (2006), Dynamics of thermochemical plumes: 1. Plume formation and entrainment of a dense layer, *Geochem. Geophys. Geosyst.*, *7*, Q02006, doi:10.1029/2005GC001071.

Lowman, J. P., and G. T. Jarvis (1995), Mantle convection models of continental collision and breakup incorporating finite thickness plates, *Phys. Earth Planet. Inter.*, *88*, 53–68.

Lowman, J. P., S. D. King, and C. W. Gable (2001), The influence of tectonic plates on mantle convection patterns, temperature and heat flow, *Geophys. J. Int.*, *146*, 619–636.

Lowman, J. P., S. D. King, and C. W. Gable (2003), The role of the heating mode of the mantle in intermittent reorganization of the plate velocity field, *Geophys. J. Int.*, *152*, 455–467.

Mitrovica, J. X. (1996), Haskell [1935] revisited, *J. Geophys. Res.*, *101*, 555–569.

Mitrovica, J. X., and A. M. Forte (1997), Radial profiles of mantle viscosity: Results from the joint inversion of convection and postglacial rebound observations, *J. Geophys. Res.*, *102*, 2751–2769.

Monnereau, M., and S. Quéré (2001), Spherical shell models of mantle convection with tectonic plates, *Earth Planet. Sci. Lett.*, *184*, 575–587.

Ogawa, M. (2003), Chemical stratification in a two-dimensional convecting mantle with magmatism and moving plates, *J. Geophys. Res.*, *108*(B12), 2561, doi:10.1029/2002JB002205.

Pollack, H. N., S. J. Hurter, and J. R. Johnson (1993), Heat flow from the Earth's interior: Analysis of the global data set, *Rev. Geophys.*, *31*(3), 267–280.

Silver, P. G., R. W. Carlson, and P. Olson (1988), Deep slabs, geochemical heterogeneity, and the large scale structure of mantle convection: Investigation of and enduring paradox, *Annu. Rev. Earth Planet. Sci.*, *16*, 477–541.

Stein, C., J. Schmalzl, and U. Hansen (2004), The effect of rheological parameters on plate behavior in a self-consistent model of mantle convection, *Phys. Earth Planet. Inter.*, *142*, 225–255.

Tackley, P. J. (1998), Self-consistent generation of tectonic plates in three-dimensional mantle convection, *Earth Planet. Sci. Lett.*, *157*, 9–22.

Tackley, P. J., and S. D. King (2003), Testing the tracer ratio method for modeling active compositional fields in mantle convection simulations, *Geochem. Geophys. Geosyst.*, *4*(4), 8302, doi:10.1029/2001GC000214.

Tackley, P. J., and S. Xie (2002), The thermochemical structure and evolution of Earth's mantle: Constraints and numerical models, *Philos. Trans. R. Soc. London, Ser. A*, *360*, 2539–2606.

Tan, E., M. Gurnis, and L. Han (2002), Slabs in the lower mantle and their modulation of plume formation, *Geochem. Geophys. Geosyst.*, *3*(11), 1067, doi:10.1029/2001GC000238.

Trompert, R., and U. Hansen (1998), Mantle convection simulations with rheologies that generate plate-like behavior, *Nature*, *395*, 686–689.

Turcotte, D. L., and G. Schubert (2002), *Geodynamics*, 456 pp., Cambridge University Press, Cambridge, U.K.

Vangelov, V. I., and G. T. Jarvis (1994), Geometrical effects of curvature in axisymmetrical spherical models of mantle convection, *J. Geophys. Res.*, *99*, 9345–9358.

van Keken, P. E. (2001), Cylindrical scaling for dynamic cooling models of the Earth, *Phys. Earth Planet. Inter.*, *124*, 119–130.

van Keken, P. E., S. D. King, H. Schmeling, U. R. Christensen, D. Neumeister, and M.-P. Doin (1997), A comparison of methods for the modeling of thermochemical convection, *J. Geophys. Res.*, *102*(B10), 22,477–22,495.

van Keken, P. E., E. H. Hauri, and C. J. Ballentine (2002), Mantle mixing: The generation, preservation, and destruction of chemical heterogeneity, *Annu. Rev. Earth Planet. Sci.*, *30*, 493–525.

van Thienen, P., A. P. van den Berg, and N. J. Vlaar (2004), Production and recycling of oceanic crust in the early Earth, *Tectonophysics*, *386*, 41–65.

Xie, S., and P. J. Tackley (2004), Evolution of U-Pb and Sm-Nd systems in numerical models of mantle convection and plate tectonics, *J. Geophys. Res.*, *109*, B11204, doi:10.1029/2004JB003176.

Zhong, S., and M. Gurnis (1994), Role of plates and temperature-dependent viscosity in phase change dynamics, *J. Geophys. Res.*, *99*(B8), 15,903–15,917.

Zhong, S., M. T. Zuber, L. Moresi, and M. Gurnis (2000), Role of temperature-dependent viscosity and surface plates in spherical shell models of mantle convection, *J. Geophys. Res.*, *105*(B5), 11,063–11,082.